

Turbulence wall-shear stress sensor for the atmospheric surface layer

This article has been downloaded from IOPscience. Please scroll down to see the full text article.

2005 Meas. Sci. Technol. 16 1644

(<http://iopscience.iop.org/0957-0233/16/8/015>)

View [the table of contents for this issue](#), or go to the [journal homepage](#) for more

Download details:

IP Address: 128.250.144.147

The article was downloaded on 23/10/2012 at 05:12

Please note that [terms and conditions apply](#).

Turbulence wall-shear stress sensor for the atmospheric surface layer

Weston D C Heuer and Ivan Marusic

Department of Aerospace Engineering and Mechanics, University of Minnesota,
Minneapolis, MN 55455, USA

Received 7 April 2005, in final form 15 May 2005

Published 11 July 2005

Online at stacks.iop.org/MST/16/1644

Abstract

A new sensor is described for measuring the fluctuating component of the wall-shear stress in the atmospheric surface layer over relatively smooth uniform terrain. The sensor was tested at the Surface Layer Turbulence and Environmental Science Test (SLTEST) site on the western salt flats of Utah, giving the first ever direct measurements of this quantity in an atmospheric-scale flow. The device consists of a lightweight floating element whose position is detected using a spherical mirror which deflects a laser beam onto a duo-lateral position-sensing photodiode. The sensor has a frequency response of 25 Hz and a circular sensing area of 50 mm diameter, making it suitable for atmospheric-scale measurements. Preliminary cross-correlation of wall-shear stress and velocity, from simultaneously sampled sonic anemometers, indicates structure-inclination angles that are consistent with analogous laboratory-scale turbulent boundary-layer measurements.

Keywords: wall-shear stress, skin-friction measurement, fluctuating surface shear stress, atmospheric boundary layer, atmospheric surface layer

(Some figures in this article are in colour only in the electronic version)

1. Introduction

Wall-shear stress, or skin friction, is the local tangential force per unit area exerted on a body as a result of fluid flow over the body. The shear stress is manifested through the ‘boundary layer’ that exists whenever there is fluid flow past a solid surface. The boundary layer comes about from the no-slip condition at the wall and is the region of high shear between the wall and the outer free-stream flow. To a great extent, the behaviour of the boundary layer determines the performance of aerodynamic surfaces such as wings, propellers and fans. The practical importance of wall turbulence has seen it to be an active area of research for the past 100 years [1]. Of fundamental importance to this problem is the need to understand the behaviour of the wall-shear stress, denoted here by τ_0 .

The accurate measurement of τ_0 has long been a challenge. Most existing techniques, as reviewed by Fernholz *et al* [2], Alfredsson *et al* [3] and Winter [4], concern the measurement of the mean, or long-time averaged, wall-shear stress. This in itself is of great importance. For example, there is debate

within the turbulence community as to what the correct form of the scaling laws for the mean velocity field should be (i.e. log law, power law or some other formulation)—see, for example, Barenblatt and Chorin [5], George and Castillo [6], Osterlund *et al* [7] and Zagarola and Smits [8]. This controversy would most likely be resolved if we could measure mean wall-shear stress to within 0.5% accuracy in existing high-quality laboratory facilities. Presently, the best techniques can only measure mean wall-shear stress to within approximately 2% accuracy.

Apart from mean, or long-time averaged, wall-shear stress, the need also exists for measuring the turbulent (fluctuating) wall-shear stress component. One important application relying on instantaneous measurements of τ_0 is large-eddy simulation (LES) of wall turbulence. In LES, the spatially filtered equations of motion, the Navier–Stokes equations, are numerically solved for a coarse computational grid and the unresolved components of the flow are modelled. For boundary layers at high Reynolds number, near-wall models are also required [9]. Many of the most popular near-wall models, particularly in the meteorological community, are

based on mean flow similarity and correlate wall-shear stress with the instantaneous velocity field at the location of the first grid point above the wall. Marusic, Kunkel and Porte-Agel [10] performed wind-tunnel tests of several near-wall models by using a rake of hot wires mounted above a spatial array of hot-film wall-shear stress probes. One of the main limitations of such studies is the uncertainty of whether the same scaling behaviour and comparisons will hold at high Reynolds number, typical of practical applications.

Over the past decade, a unique facility has been developed on the western Utah salt flats by Klewicki and co-workers [11, 12] to study ‘laboratory-like’ high Reynolds number flows using a geophysical environment. The Surface Layer Turbulence and Environmental Science Test (SLTEST) facility is located on extremely flat and barren salt flats that extend over 240 km north–south and 48 km east–west. The facility provides an excellent location to test near-wall models of LES and other boundary-layer phenomena.

The original motivation for the present study was to develop a sensor capable of measuring the time series of wall-shear stress in the atmospheric surface layer at SLTEST and use it for LES near-wall model studies. One particular advantage of making measurements at SLTEST is having a flow with large temporal and spatial turbulence eddy scales. This means that the spatial resolution is easily achieved, and instruments with a frequency response of nominally 25 Hz (such as a sonic anemometer) can capture the dominant energetic scales in the flow. The main disadvantages of making measurements at SLTEST are having to make measurements in a harsh environment, as well as having typically very small signals. For example, a typical wall-shear stress encountered at SLTEST is $\tau_0 = 0.05$ Pa. For a sensor with a circular sensing area of 50 mm diameter, this requires the measurement of a force of nominally $100 \mu\text{N}$. Such requirements make the development of a reliable device a non-trivial exercise.

Sadr and Klewicki [13] have made measurements of mean wall-shear stress at SLTEST using a floating-element device with micro force transducers. Their plate was 2 m in diameter and therefore is only suitable for average measurements. Thermal-based systems such as hot films and hot wires are not suitable for various practical reasons due to their fragility and need for extensive temperature-sensitive calibration. The final design chosen, that is presented here, is based on a floating-element principle using an optical-laser technique to infer the shear forces. Details of the sensor design, calibration and sample measurements at SLTEST are presented in the remainder of the paper.

2. Floating-element sensor design

There are several ways to construct a floating-element sensor, each of which has its own advantages and disadvantages. The design parameters of concern are high frequency, device stability, degree of robustness and ease of use. Many previous devices have been optimized for measuring mean wall shear and device stability, but the present design was chosen as a compromise to the above requirements, in addition to being simple in construction and easy to analyse.

The sensing element is a lightweight flat plate made of Styrofoam supported by four stainless steel wires. Advantages

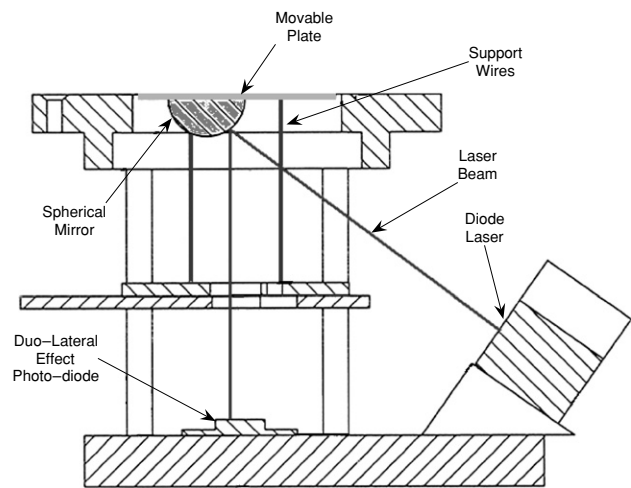


Figure 1. Details of the sensor.

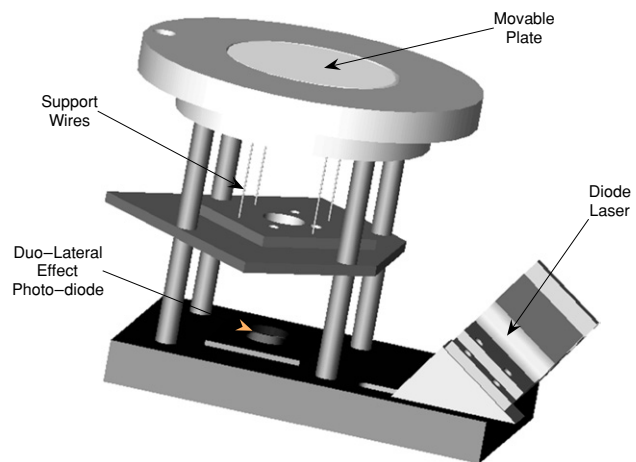


Figure 2. Sketch of the sensor.

to this type of construction are several, namely the plate is kept level upon deflection from the wall-shear stress, the choice of material allows wall-shear stress measurements to be made at relatively high frequencies and with high sensitivity, and finally, simple components make the final output predictable. A schematic of the sensor is shown in figure 1. Figure 2 shows a three-dimensional sketch of the final sensor with component labels included for clarity.

Owing to small displacements, the system may be analysed as a simple spring and mass system with a few caveats. The maximum frequency that may be resolved is determined by the resonance frequency equation

$$f = \frac{1}{2\pi} \sqrt{\frac{k_{\text{eq}}}{m_{\text{eq}}}}. \quad (1)$$

Here, k_{eq} is the equivalent spring constant and m_{eq} is the equivalent mass for the system, as in Rao [14] (details of how m_{eq} is determined are given in section 3.) The other important relation for the sensor is the size of the displacement that must be measured for an applied τ_0 given by

$$x = \frac{\tau_0 A}{k_{\text{eq}}}, \quad (2)$$

where A is the surface area of the top of the plate. Note the dependence in both equations (1) and (2) on k_{eq} . If

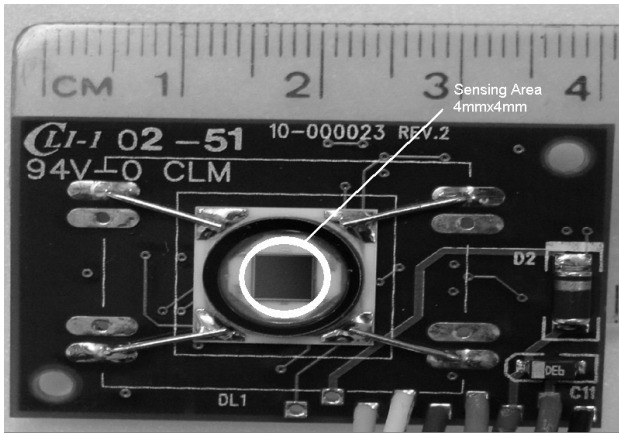


Figure 3. Close-up of the position detector sensing area.

k_{eq} is increased to increase the resonance frequency, the corresponding displacement for a given τ_0 will decrease, thereby reducing the sensitivity of the sensor. To maintain a measurable displacement and a resonance frequency high enough, the only variable remaining is m_{eq} . By making the plate and other components out of the lightest material possible, thus the choice of Styrofoam, it is possible to achieve both design goals simultaneously.

For the corresponding design, the resonance frequency was calculated to be 21 Hz and this was compared to an estimate of 23 Hz from a finite-element simulation, both of these estimates being slightly conservative. An experimental test of the sensor showed the actual measured resonance frequency to be 29 Hz, which is above the minimal desired response.

The chief obstacle in the design of the sensor is detecting the movement of the plate, the fluctuating motion being of the order of 10 μm and mean displacement of roughly 100 μm . After investigating several methods, the present design was chosen. The method of operation is to reflect a laser beam off a spherical mirror attached to the bottom of the moving plate onto a duo-lateral position-sensing photodiode with a resolution of 0.25 μm . The spherical mirror is a thin plastic dome with a highly reflective surface coating.

Detection of the laser beam is accomplished with a Pacific Sensor DL16-7PCBA duo-lateral photodiode detector. A detector of this type works by determining the two-dimensional position of the laser spot centroid on the detector and outputting a proportional voltage. Figure 3 shows the detector along with the sensing area highlighted. In addition to the positional voltages, a voltage proportional to the light intensity along each axis is output as well, which is used to normalize the position voltage. The voltage output from the positional channel is dependent on incident laser power and must be normalized to account for this variation. Figure 4 shows the signal path for the detector including a 25 Hz low-pass filter to eliminate aliasing and resonance effects. The voltage proportional to movement in one direction is denoted by x and the intensity signal in that direction is denoted as x_{int} , with the normalized signal denoted as x_{norm} . Similar notation is used for the orthogonal direction. Signal normalization was performed in post-processing.

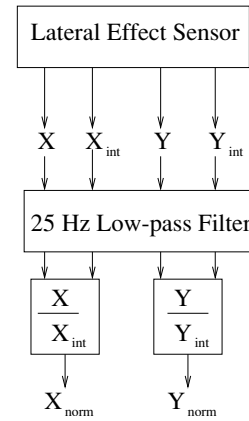


Figure 4. Signal path from the position detector.

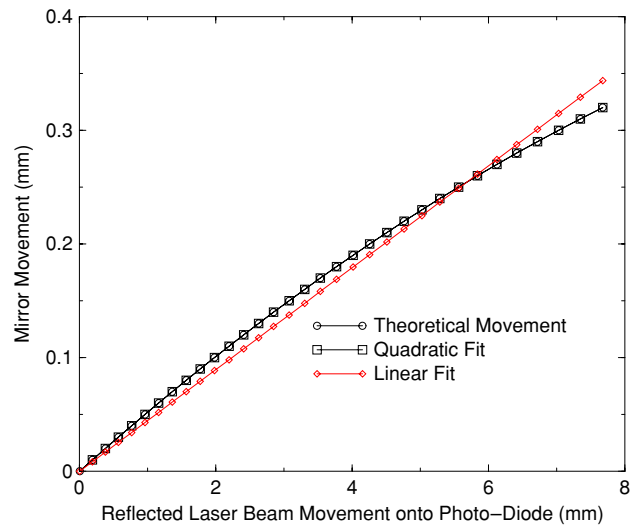


Figure 5. Theoretical reflected laser beam movement due to a spherical mirror.

In order to resolve the two-dimensional movement of the plate, the laser is reflected off a spherical mirror. This does however introduce a non-linearity in the relationship of the plate position and the incident laser position on the photodiode, which must be modelled. A simple ray analysis suggests the relationship to be governed by trigonometric functions, and over the range of the plate movement expected it is well approximated by a quadratic curve fit as shown by the estimated theoretical curves in figure 5. This same effect is also seen in the final calibration, discussed in the next section. A given plate deflection yields a greater corresponding displacement of the reflected laser beam on the photodiode, due to the three-dimensional (nominally spherical) shape of the mirror, combined with the large separation distance between the mirror and photodiode. For the actual sensor, the amplification factor was approximately 7. This amplification, of course, effectively increases the sensitivity of the laser detector and the sensor as a whole.

3. Calibration

The major challenge for calibrating the sensor was in generating a reference force, which must be parallel to the

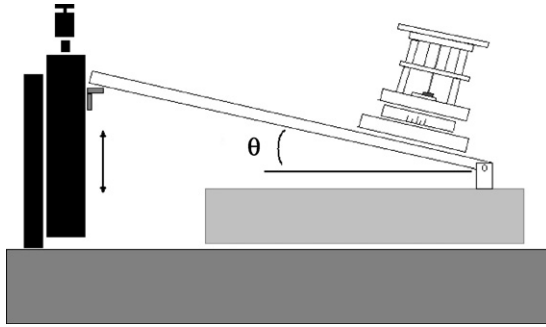


Figure 6. Calibration rig. The length of the tilting plate is 610 mm and the vertical traverse has a stepping increment of 1.27 μm .

plate and small in magnitude. This was overcome by using a tilting plate calibration rig as shown in figure 6. As the angle of the tilting plate changes, more of the weight force is resolved in the direction parallel to the plate. Small changes in the force normal to the plate are expected to have a negligible effect, owing to the geometry of the structure of the plate supports. The angular adjustment of the plate is achieved by a computer-controlled stepper motor with very fine angular adjustment.

One parameter which needs to be determined after the sensor is assembled, is the effective mass of the plate. This was determined by moving the tilting plate to a fixed angle and recording the output voltage at this angular position. A known mass is then added to the moving plate and the tilting plate is adjusted until it matches the previous output voltage. A static equation is then solved with the two angles and the only unknown being the mass of the moving plate. This procedure is repeated several times at different angles and a best fit of the mass of the plate is obtained. We estimate the uncertainty in m_{eq} to be approximately 3%.

The calibrations of the span-wise and stream-wise directions are the same except in the range of wall-shear stress, τ_0 , that is applied during the calibration. The span-wise direction is calibrated from -4.2° to 4.2° , a variation of -0.1 to 0.1 Pa, because the shear levels are expected to be both positive and negative near zero. The stream-wise calibration varies from 0° to 8.4° , a variation of 0 to 0.2 Pa, because the stream-wise direction will only have shear in the positive direction and has a non-zero mean.

When the sensor is level, no shear force is simulated and this is used as the reference point for the rest of the calibration. The data acquisition system and the tilting plate control system are linked by an external trigger, so data acquisition and the movement of the tilting plate are synchronized. The tilting plate moves at a fixed continuous rate between the reference and the calibration angle limits. The movement of the tilting plate is converted to shear stress by a static equation based on the weight of the sensor plate, as determined previously, and the angle of the tilting plate. In post-processing, the direction voltage is normalized by the intensity, as described earlier. The final step is to curve fit the data to obtain a calibration curve, shown in figures 7 and 8.

Over a long time period, a dc shift in the output voltage was detected that is not a result of the wall-shear stress, and this would need to be addressed for use in the field. The current hypothesis is that the drift has a mechanical origin,

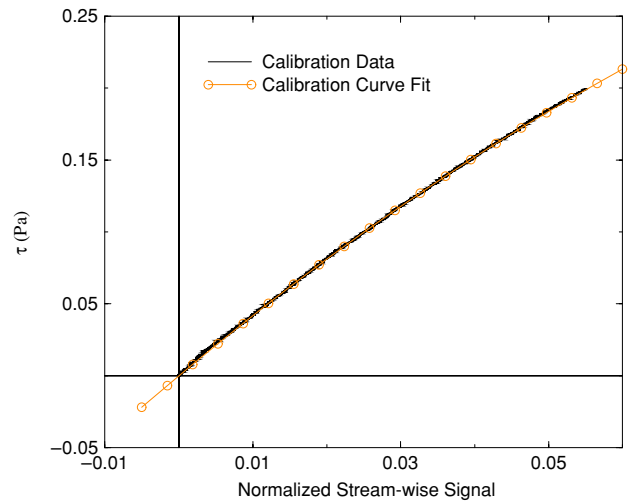


Figure 7. Stream-wise calibration.

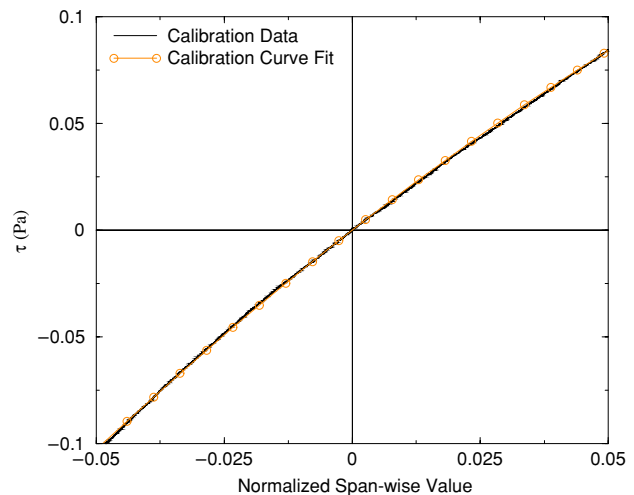


Figure 8. Span-wise calibration.

by temperature effects or other means. For the present measurements at SLTEST, this is not a problem because in these experiments the mean shear can be estimated using another method, and the main purpose of this sensor is to obtain the fluctuating component of the wall-shear stress. The mean shear stress was estimated using sonic anemometers to obtain the Reynolds shear stress, which for atmospheric surface layer flows is regarded as a good approximation for $\langle \tau_0 \rangle / \rho$, where the angled brackets denote a mean value and ρ is the density of air. From this estimate of $\langle \tau_0 \rangle$, the drift can be corrected. However, the dc shift would cause a fairly serious bias error if an experiment was conducted where there is not another method to determine the mean wall-shear stress. This dc shift issue is under further investigation.

4. Preliminary results from field trials

The sensor was tested in the atmospheric surface layer (ASL) at the SLTEST site in May 2004. The experiment had two objectives: first to determine how the sensor would function in the field, and second to investigate the large-scale information

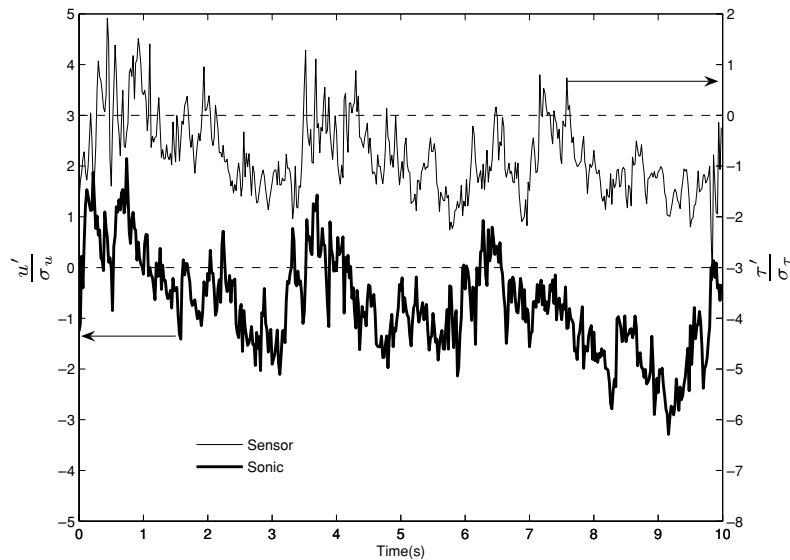


Figure 9. Close-up of normalized signal compared to stream-wise velocity signal from a sonic anemometer positioned 0.24 m above the sensor.

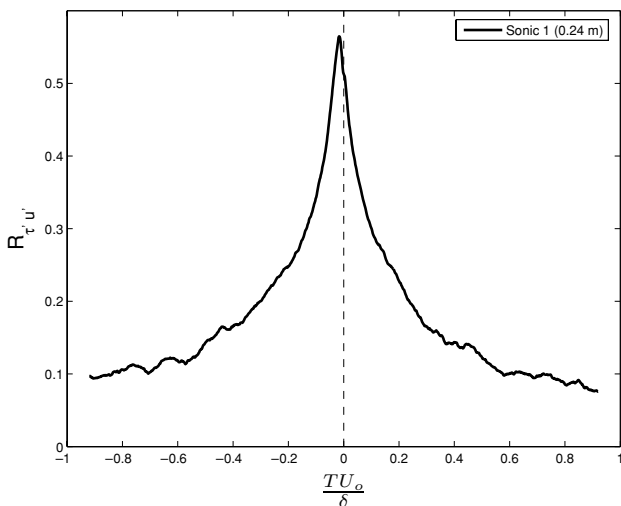


Figure 10. Cross-correlation between the sensor and u velocity signal from the sonic anemometer positioned 0.24 m above the sensor.

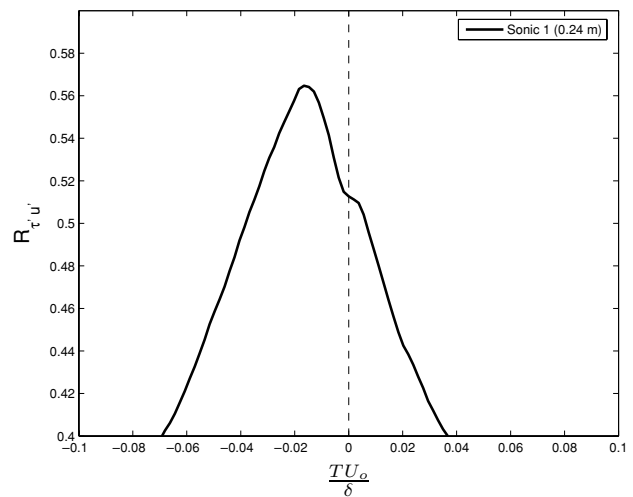


Figure 11. Close-up of peak shown in figure 10.

that is contained in the ASL and compare these data to previous low Reynolds number laboratory experiments, such as that of Brown and Thomas [15].

The setup for this experiment included five sonic anemometers that yield all three directions of velocity as well as temperature. These were arranged in a logarithmically spaced vertical array from 0.24 m to 2.92 m above the wall-mounted sensor. The data presented came from a time period where the flow would be considered near-neutral by meteorological criteria ($z/L = -0.02$, where z is the wall normal location of the sonic anemometer and L is the Monin–Obukhov length, a ratio of mechanical shear to the buoyancy effects, see Stull [16]). The remaining relevant conditions for this experiment are the wall-shear velocity $u_\tau = 0.28 \text{ m s}^{-1}$ and estimated outer parameters $U_0 = 11.2 \text{ m s}^{-1}$ with $\delta = 100 \text{ m}$.

The data presented are from the wall-shear stress sensor and the first sonic anemometer in the array. An expanded view

of 10 s of data is shown in figure 9. Note that both signals are normalized by their standard deviations to allow the signals to be plotted on similar axis. Items of note are that time delay between the sensor and the sonic anemometer can be seen, and the overall trend is quite similar between the two signals.

Figures 10 and 11 show the cross-correlation between the sensor and the sonic anemometer, where a couple of interesting items can be determined. Firstly, there is a strong correlation between the two instruments witnessed by the peak correlation value of 0.57. Also, there is a phase lag between the two signals, and the average physical angle between these signals is 14.2° to the horizontal at $z/\delta = 0.0024$, based on the mean velocity at that sonic height. This time delay can be thought of as an inclination angle of a large coherent motion seen by the sonic anemometer and the wall-shear stress sensor. This compares favourably with the results from Brown and Thomas [15], where they found it to be an average of 18° over the entire boundary layer.

5. Conclusions

An instrument was designed and tested that has the capability to measure a time series of wall-shear stress fluctuations in the atmospheric surface layer. Field tests were successfully carried out at the SLTEST site on salt flats in Utah. The sensor achieved the desired frequency response of 25 Hz and was able to continuously measure the fluctuating wall-shear stress autonomously over a long sampling period (several days), without encountering a system failure in this harsh environment. The accuracy of measured fluctuating shear stress is estimated to be better than 5%. One limitation of the present device is that, due to dc drift, an independent device for measuring the mean wall-shear stress is required. The dc drift is believed to be caused by mechanical thermal expansion and future efforts will go towards eliminating this.

In the Utah experiments, simultaneous measurements were also made of fluctuating velocity using sonic anemometers. Under neutrally buoyant conditions, cross-correlations between fluctuating wall-shear stress and stream-wise velocity, at various heights above the sensor, compare very favourably with previous laboratory results. This suggests that these cross-correlation functions are Reynolds number invariant over three orders of magnitude change in Reynolds number. However, these results should be regarded as preliminary and are the focus of continuing work.

Acknowledgment

The authors wish to gratefully acknowledge the financial support of the David and Lucile Packard Foundation.

References

- [1] Lumley J L and Yaglom A M 2001 A century of turbulence flow *Flow Turbul. Combust.* **66** 241–86
- [2] Fernholz H H, Janke G, Schober M, Wagner P M and Warnack D 1996 New developments and applications of skin-friction measuring techniques *Meas. Sci. Technol.* **7** 1396–409
- [3] Alfredsson P K, Johansson A V, Haritonidis J H and Eckelmann H 1988 The fluctuating wall-shear stress and the velocity field in the viscous sublayer *Phys. Fluids* **31** 1026–33
- [4] Winter K G 1977 An outline of the techniques available for the measurement of skin friction in turbulent boundary layers *Prog. Aerospace Sci.* **18** 1–57
- [5] Barenblatt G I and Chorin A J 1998 Scaling of the intermediate region in wall-bounded turbulence: the power law *Phys. Fluids* **10** 1043–4
- [6] George W K and Castillo L 1997 Zero-pressure-gradient turbulent boundary layer *Appl. Mech. Rev.* **50** 689–729
- [7] Osterlund J M, Johansson A V, Nagib H M and Hites M H 2000 A note on the overlap region in turbulent boundary layers *Phys. Fluids* **12** 1–4
- [8] Zagarola M V and Smits A J 1998 Mean-flow scaling of turbulent pipe flow *J. Fluid Mech.* **373** 33–79
- [9] Piomelli U and Balaras E 2002 Wall-layer models for large-eddy simulations *Ann. Rev. Fluid Mech.* **34** 349–74
- [10] Marusic I, Kunkel G and Porte-Agel F 2001 Experimental study of wall boundary conditions for large eddy simulations *J. Fluid Mech.* **446** 309–20
- [11] Klewicki J C, Foss J F and Wallace J M 1998 High Reynolds number [$Re_\theta = o(10^6)$] boundary layer turbulence in the atmospheric surface layer above western Utah's salt flats *Flow at Ultra-High Reynolds and Rayleigh Numbers* ed R J Donnelly and K R Sreenivasan (Berlin: Springer) pp 450–66
- [12] Metzger M M and Klewicki J C 2001 A comparative study of near-wall turbulence in high and low Reynolds number boundary layers *Phys. Fluids* **13** 692–701
- [13] Sadr R and Klewicki J C 2000 Surface shear stress measurement system for boundary layer flow over a salt playa *Meas. Sci. Technol.* **11** 1403–13
- [14] Rao S S 1995 *Mechanical Vibrations* 3rd edn (Reading, MA: Addison-Wesley)
- [15] Brown G L and Thomas A S W 1977 Large structure in a turbulent boundary layer *Phys. Fluids* **20** S243–52
- [16] Stull R B 1997 *An Introduction to Boundary Layer Meteorology* (Dordrecht: Kluwer)